**Proceedings of the ASME 2013 Conference on Smart Materials, Adaptive Structures and Intelligent Systems**
**SMASIS2013**
**September 16-18, 2013, Snowbird, Utah, USA**

# SMASIS2013-3206

# SPEED OF SOUND MEASUREMENT IN SOLIDS USING POLYVINYLIDENE FLUORIDE (PVDF) SENSORS

**Leon M. Headings** **Kunal Kotian** **Marcelo J. Dapino**
**The Ohio State University, Department of Mechanical and Aerospace Engineering, Columbus, Ohio, USA**

## ABSTRACT

Piezoelectric film sensors such as polyvinylidene flouride (PVDF) generate an electrical voltage in response to an applied mechanical stress with a remarkably high sensitivity. They provide very fast response times and do not require extensive signal conditioning. This paper presents a straightforward method of measuring the speed of sound in solid materials and structures using commercial PVDF sensors.

PVDF sensors are most commonly used to measure stresses applied in the sensors' thickness direction. However, this requires that the sensors be located in the load path, which may result in damage to the sensor or affect the response of the system. In this paper, two PVDF sensors are bonded to the side of a structure and a small impact is applied to one end. The sensors are used to measure the time for the impact-induced plane stress wave to travel between the sensors. The observed speed of the propagating stress wave is shown to be in good agreement with the theoretical speed of sound for the material and finite element calculations. In addition, the finite element simulations confirm the validity of the plane wave assumption for non-ideal and non-uniform impact inputs.

## INTRODUCTION

Polyvinylidene flouride (PVDF) is a durable, compliant polymer which exhibits piezoelectric properties in its beta phase. Thus, it can be used as a sensor that generates charge in response to an applied stress or as an actuator that produces strain in response to an applied electric field. PVDF is available in the form of inexpensive films and exhibits a high stress sensitivity. Since a PVDF sensor converts mechanical energy into electrical energy, it can often be used without external power or sophisticated circuitry.

Piezoelectrics are commonly used to measure the speed of sound of materials using pulse-echo techniques. In general, a piezoelectric transducer is used to transmit one or more ultrasonic pulse inputs to the specimen either directly or through another medium such as a fluid bath. The transmitting transducer and/or additional receiving transducers are used to record the pulse after it reflects or passes through the specimen. The speed of sound is then calculated based on time-of-flight calculations or frequency-domain analyses.

Piezoceramics such as lead zirconate titanate (PZT) are commonly used for ultrasound measurements because the force output of PVDF is too low to act as an ultrasound transmitter in many applications. However, PVDF is used in some cases where its acoustic impedance is a better match than PZT with mediums such as fluid baths, for example.

A wide variety of configurations and techniques have been developed for measuring the speed of sound in different materials. In the simplest case, a transducer applies an ultrasonic pulse to one face of a solid material and a separate sensor measures the resulting pulse on the opposite face. The speed of sound is then calculated based on the time-of-flight and the known distance between the transmitter and the receiver. The accuracy of the speed of sound measurement may be limited by the accuracy of the thickness measurement.

For biological specimens, it is difficult to measure thickness accurately; Kuo et al. [1] introduced a method using a transducer (acting as both a transmitter and a receiver) and receiver at a known distance apart in a fluid bath, with the specimen placed between them. The speed of sound in the specimen can be calculated based on the times-of-flight of reflections back to the transducer from the front and back faces of the specimen, the times-of-flight from the transducer to the receiver with and without the specimen in place, and the known speed of sound in the fluid bath. The calculation does not require knowledge of the specimen thickness or the location of the specimen between the transducer and receiver. An alternate configuration was presented where the receiver could be replaced by a reflector. Hsu and Hughes [2] further developed this method and were able to deduce the specimen thickness for composite laminates. This test configuration was later used by He [3] who determined the speed of sound and sample thickness based on the phase spectra of the four signals. While

 

these methods require the sample to be submerged and access to both sides, Hsu et al. [4] presented a method for calculating the speed of sound, plate thickness, and wedge angle between the top and bottom surfaces using direct-contact transducers on only one side of the object.

Most speed of sound measurement techniques rely on the use of a transmitter to apply one or more short stress pulse inputs. In contrast, the method described in this paper uses a stress input which is applied using an impact hammer. Because the time-of-flight is determined from the difference in times at which the stress wave front reaches the two PVDF sensors, the exact force profile of the input is not important and does not need to be recorded. Unlike stress inputs from transducers, the force input from an impact hammer has a much longer duration. While this type of impact input for measuring the speed of sound has not been reported, PVDF has been used to measure various types of impacts and shock waves.

Obara et al. [5] designed an inexpensive PVDF sensor which was used to measure the response to a shock wave caused by the impact of a polymethyl methacrylate (PMMA) projectile traveling at 460 m/s on a PMMA target. Zhu et al. [6] used PVDF sensors to measure laser-induced shock waves and recorded the pressure history for foils confined by PMMA. The sensor output showed reverberations of the shock wave within the foil and was compared with the results of analytical models. Although most laser-induced shock testing uses pulses in the range of 20-30 ns, Peyre et al. [7] used PVDF for laser-induced shock testing at pulse widths down to 0.6 ns. The sensor accurately measured the shock wave profile up to a laser intensity of 160 GW/m$^2$ in a water-confined regime. Bauer [8] tested PVDF film under impact loads up to 25 GPa and showed that the sensor's response was independent of the loading path. In all of the shock wave stress measurements cited above, the PVDF sensor was used to sense stresses applied in the thickness direction (33 mode) and demonstrated response times on the order of nanoseconds.

PVDF sensors are most commonly used to measure stresses applied in the thickness direction (33 mode), but are also quite effective at sensing stresses in the longitudinal direction (31 mode). The 31 mode is used when a PVDF sensor is bonded to beams or structures such that bending or transverse stress waves create longitudinal stresses in the sensor. For the speed of sound measurement technique described in this paper, an impact hammer is used to apply a stress input at the end of a structure such that compression stress waves travel along the length of the structure. These plane stress waves result in longitudinal stresses (31 or 32 mode) in two PVDF sensors bonded at different locations along the side of the structure. The speed of sound in the material is consequently calculated using the known distance between the sensors and the difference in times at which the stress wave front reaches the two sensors. Experimental test results are compared against the theoretical speed of sound and finite element models are used to simulate the speed of sound and examine the effects of non-ideal and non-uniformly applied impacts.

## NOMENCLATURE

| | *Description* | *SI Unit* |
|---|---|---|
| $D$ | electric displacement | C/m$^2$ |
| $E$ | electric field | V/m |
| $G$ | shear modulus (rod) | Pa |
| $S$ | strain (PVDF) | - |
| $T$ | stress (PVDF) | Pa |
| $V$ | voltage | V |
| $Y$ | elastic modulus (rod) | Pa |
| $c$ | speed of sound, analytical calculation | m/s |
| $c_{exp}$ | speed of sound, experimental testing | m/s |
| $c_t$ | speed of sound, transverse waves | m/s |
| $g$ | piezoelectric voltage constant | Vm/N |
| $h$ | thickness (PVDF) | m |
| $r$ | radius (rod) | m |
| $s^D$ | compliance, measured at $D$=0 (PVDF) | 1/Pa |
| $t_1$, $t_2$ | time instants, stress wave reaches sensors | s |
| $t_t$ | stress wave transit time | s |
| $x_t$ | transit distance, sensor leading edges | m |
| $\beta^T$ | impermittivity, measured at $T$=0 (PVDF) | m/F |
| $\rho$ | density (rod) | kg/m$^3$ |

## PVDF SENSING OF PLANE STRESS WAVES

Piezoelectric materials such as PVDF can be modeled using the following strain-field formulation of the linearized coupled constitutive equations:

$$S_p = s^D_{pq} T_q + g_{kp} D_k, \tag{1}$$

$$E_i = g_{iq} T_q + \beta^T_{ik} D_k. \tag{2}$$

Here, $S$ is strain, $T$ is stress, $E$ is electric field, $D$ is electric displacement, $s^D$ is compliance measured at zero electric displacement, $g$ is the piezoelectric voltage constant, and $\beta^T$ is the impermittivity measured at zero stress. The vector subscripts $i$ and $j$ have values of 1, 2, and 3. The compressed tensor subscripts $p$ and $q$ have values of 1, 2, 3, 4, 5, and 6, corresponding to 11, 22, 33, 12, 23 or 32, 31 or 13, and 12 or 21, respectively. As shown in Figure 1, the values 1, 2, and 3 designate the length, width, and thickness directions of the sensor, respectively, with the 3-direction being the typical axis of polarization.

When the PVDF sensor output is measured by a device with an infinitely high input resistance the sensor acts as an open circuit. Thus, the electric displacement $D$ is zero and the piezoelectric equations are decoupled. Recognizing that $E_3$=$V$/$h$, where $V$ is voltage across the electrodes and $h$ is the thickness of the PVDF film, the PVDF output voltage can then be written from (2) as

$$V = h g_{31} T_1 + h g_{32} T_2 + h g_{33} T_3. \tag{3}$$

Thus, the piezoelectric coefficients $g_{31}$, $g_{32}$, and $g_{33}$ relate the voltage generated in the direction of polarization (3 direction) due to stresses in the 1, 2, and 3 directions, respectively. The 33 mode, where stress is applied in the thickness direction, provides the greatest sensitivity and is the most commonly used

mode for PVDF sensors. While this is the mode that has been typically used in the literature for shock and impact measurements, it has the disadvantage of needing to be located in the load path. In addition to being susceptible to damage, the sensor is likely to affect the response of the system to an impact or other type of input. Therefore, this paper focuses on the use of PVDF film sensors on the sides of structures to measure plane stress waves using the 31 or 32 modes.

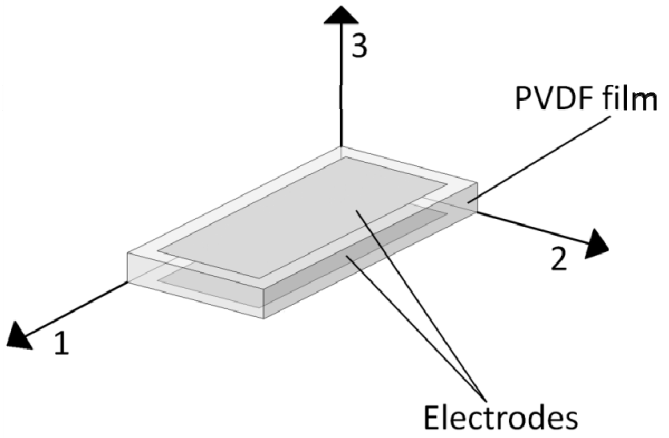


**Figure 1. Diagram of PVDF sensor's axes.**

For one-dimensional stress wave propagation, it is assumed that there is a uniaxial state of stress in the structure. For an impact response, the impact is assumed to apply a uniform compressive stress on one end of the structure. This compressive stress travels along the length of the rod as a plane stress wave [9]. Then, as long as this plane stress wave assumption is valid, the speed of sound $c$ for impact-induced longitudinal plane stress waves can be written as

$$c = \sqrt{\frac{Y}{\rho}}, \tag{4}$$

where $Y$ is the elastic modulus and $\rho$ is the density of the material. The analysis in this paper is based on the following assumptions:

- Stress wave propagation in the structure is one-dimensional, with stress waves that are planar.
- The structure and PVDF sensor are perfectly elastic.
- The PVDF sensor's stiffness is much lower than the stiffness of the bar, such that the sensor and adhesive do not affect stress wave propagation in the bar.
- The PVDF sensor output voltage is measured by an ideal measurement system such that the sensor can be considered in open-circuit mode and the measurement system does not affect the dynamics of the voltage measurements.

While the PVDF open circuit voltage output is related to the average stress in the sensor (3) and is sensitive enough to measure very small stresses, the charge output is relatively low. As a result, it is necessary to use a data acquisition system with a high input resistance in order minimize the effects of the electrical circuit formed by the PVDF and measurement system. This electrical circuit acts as a high pass filter with a time constant resulting primarily from the input resistance of the measurement system and the capacitance of the PVDF sensor.

Although it is assumed that the PVDF sensor is securely bonded to the structure, with the adhesive effectively transferring strain from the structure to the sensor, the experimental speed of sound measurements are based on the detection of the leading edge of the stress wave. Since the speed of sound measurement does not rely on the magnitude of stress in the bar being accurately calculated from the PVDF output voltage, it is not necessary to assume complete strain transfer. It is only critical that the dynamics of the PVDF output response are not affected by the imperfect strain transfer and that a sufficient signal-to-noise ratio can be achieved.

The elementary theory for one-dimensional plane stress wave propagation is only valid when lateral inertia effects are negligible. These effects result in a distortion of the shape of the stress wave front. The lateral inertia effects can be neglected when the duration of the impact force input is large compared to the time it takes for the stress wave to travel laterally from the center to the side of the structure [10]. For the case of a rod, the time $t_r$ for a stress wave to travel across the radius of the rod can be calculated as

$$t_r = \frac{r}{c_t} = r\sqrt{\frac{\rho}{G}}, \tag{5}$$

where $r$ is the radius of the rod, $c_t$ is the speed of propagation of the transverse (or lateral) waves, and $G$ is the shear modulus of the material.

## EXPERIMENTAL TESTING

Experimental testing was conducted in order to verify and demonstrate that PVDF patch sensors have a high enough sensitivity and response speed to measure small plane stress waves propagating through a material and determine the speed of sound in the material. The testing also demonstrates the suitability of the sensor bonding method as well as the data collection and analysis techniques.

### Experimental Setup and Methods

In order to test the use of PVDF sensors to measure the speed of sound in a solid material or structure, two PVDF sensors were attached to a 316L stainless steel rod as shown in Figure 2. The rod had a diameter of 32 mm, a length of 350 mm, and was suspended horizontally using two fishing lines. PVDF sensors manufactured by Measurement Specialties Inc., model DT1-028K, were used which have only a thin urethane coating over the silver ink electrodes. Other Mylar-coated sensors have been successfully tested on other structures, but the higher stiffness makes them more difficult to bond to curved surfaces such as the side of small a rod.

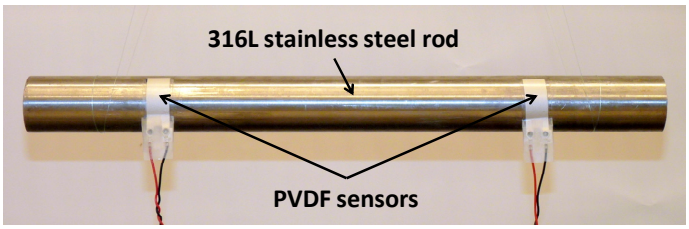


**Figure 2. Photo of suspended rod with PVDF sensors attached to measure stress wave transit time.**

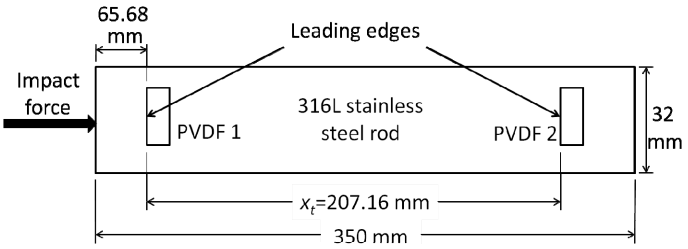


**Figure 3. Schematic of rod with PVDF sensors attached to measure stress wave transit time.**

PVDF sensors were attached at two locations along the length of the rod, as shown in Figure 3, using a thin layer of cyanoacrylate glue. The piezoelectric stress constant $g_{31}$ is much higher than $g_{32}$, so it is best to use the sensors in 31 mode. However, because the riveted attachment of the lead wires makes it difficult to conform these particular sensors to the curved bar surface, they were used in 32 mode for these tests.

An impact force was applied to one end using a piezoelectric impact hammer. The impact-induced stress wave propagates along the length of the bar and, when it reaches a PVDF sensor, the strain in the bar is transferred to the sensor. While PVDF output voltage is related to the average stress in the sensor, it begins increasing from zero as soon as the stress wave reaches the leading edge of the sensor. We define the stress wave transit time $t_t$ as the time it takes for the stress wave to travel between the leading edges of the two sensors. This is also commonly referred to as the time-of-flight. The distance between the leading edges of the two PVDF sensors was carefully measured to be $x_t$=207.16 mm Thus, the speed of sound in the material can be calculated by measuring the stress wave transit time.

To record the PVDF sensor output, a two-channel digital storage oscilloscope was used without any interfacing electronics between the sensors and the oscilloscope. The oscilloscope had a sampling frequency of 100 MHz and an input resistance of 1 MΩ. For each channel, a 9 MΩ 10x oscilloscope cable was used, for a total input resistance of 10 MΩ. A second oscilloscope of the same type was used to record the impact hammer output and the impact hammer signal was used to trigger the data acquisition for both oscilloscopes.

As discussed in the previous section, this analysis is based on the assumption of one-dimensional plane stress wave propagation, which requires that the lateral inertia effects are negligible. To evaluate whether lateral inertia effects can be neglected, the theoretical time for a stress wave to travel across the radius of the bar can be calculated using (5) for the 316L stainless bar, where $\rho$ is 8000 kg/m$^3$ and $G$ is 82 GPa. The resulting radial travel time $t_r$ is 5 μs. The impact forces recorded from the piezoelectric impact hammer for four tests are shown in Figure 4. The shortest impact lasts for approximately 120 μs, which is 24 times larger than $t_r$. Therefore, since the duration of the impact is much larger than the time for a stress wave to travel across the radius of the rod, it is reasonable to neglect lateral inertia effects and assume one-dimensional stress wave propagation for this experiment.

For 316L stainless steel, $Y$ is 193 GPa. So, using (4), the theoretical speed of sound in 316L stainless steel can be calculated as $c$ = 4912 m/s.

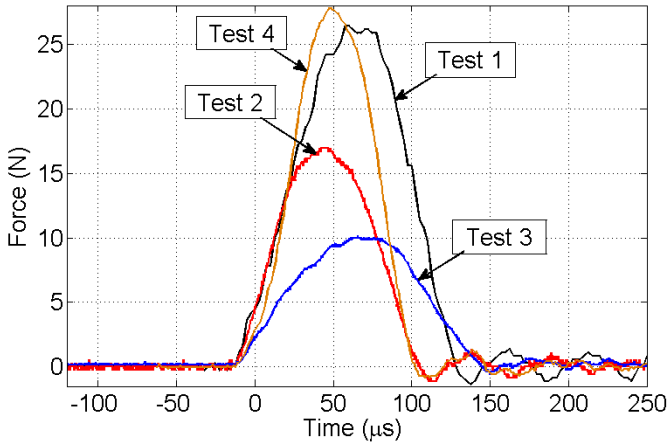


**Figure 4. Impact forces recorded by the piezoelectric impact hammer.**

## Experimental Results: Speed of Sound Measurement

Four tests were conducted and the input forces were recorded from the piezoelectric impact hammer as shown in Figure 4. A moving average with a span of 1000 elements (corresponding to 5 μs) was applied to the PVDF sensor output voltage and the sign of the voltage was inverted for plotting. The results for test 3 are shown in Figure 5 and are representative of the other tests. Using these PVDF sensor output voltage results, the following steps were followed to determine the stress wave transit time for each test:

1. The mean voltage level for each PVDF sensor before impact (i.e., before the voltage started rising) was subtracted from the full PVDF signal.

2. For each PVDF sensor, the time instants were selected at which the voltage rose above zero and did not subsequently fall below zero for at least 50 μs. These time instants $t_1$ and $t_2$ are noted in Figure 5.

3. The stress wave transit time $t_t$ was calculated as the difference between the two time instants found in step 2.

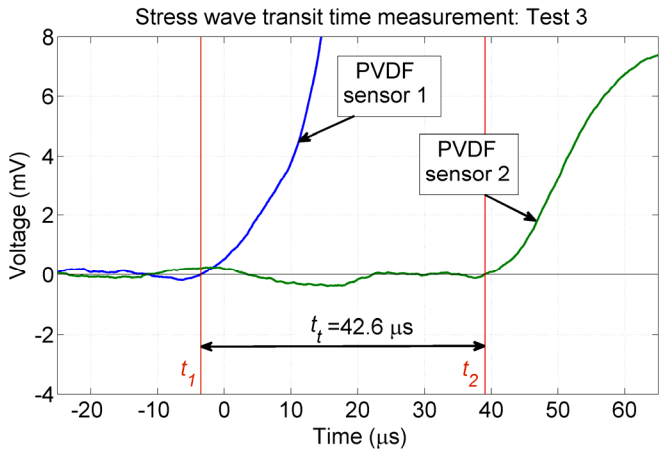


**Figure 5. Example of test results with calculated stress wave transit time.**

Using the value of the stress wave transit time $t_t$ for each test, the experimentally measured speed of sound $c_{exp}$ can be calculated as

$$c_{exp} = \frac{x_t}{t_t} = \frac{207.16*10^{-3}}{t_t}, \quad (6)$$

where $x_t$ is in meters and $t_t$ is in seconds. Table 1 summarizes the experimental speed of sound results for each test. It also shows the percentage error between the experimental and theoretical speed of sound values.

The average value of $c_{exp}$ is 4871 m/s and the percentage error between this value and the theoretically calculated $c$ is 0.8%.

**Table 1. Experimental results from three tests.**

| Test number | $c_{exp}$ [%] | Percentage error between $c_{exp}$ and $c$ |
|---|---|---|
| 1 | 4944 | 0.7% |
| 2 | 4807 | 2.1% |
| 3 | 4863 | 1.0% |
| average | 4871 | 0.8% |

## Experimental Results: Speed of PVDF Response

When two PVDF sensors are used to measure the stress wave transit time, the impact force does not need to be recorded, so the impact hammer does not need to be piezoelectric. However, for further validation of the PVDF response time, the speed of sound was also calculated using the time difference between the leading edges of the piezoelectric impact hammer's output and the output voltage of the nearest PVDF sensor. According to the manufacturer's published specifications [11], the PVDF sensor has a bandwidth of up 1 GHz, which corresponds to a measureable time resolution of 1 ns.

For test 4, Figure 6 shows the impact force and output voltage from PVDF sensor 1. The time interval between the start of the impact force and the PVDF output voltage was calculated to be 13.1 μs. The distance between the impacted end of the rod and PVDF sensor 1 was carefully measured as 65.68 mm. Thus, using these values and (6) we get the experimentally measured speed of sound $c_{exp,2}$ as 5014 m/s. The percentage error between this value and the theoretical value of speed of sound in 316L stainless steel is 2.1%. Despite being a very short time interval and stress wave travel distance, the percentage error is low. Therefore, this implies that the PVDF sensor responds quickly and does not introduce any significant time lag between the arrival of the traveling stress wave and the voltage output.

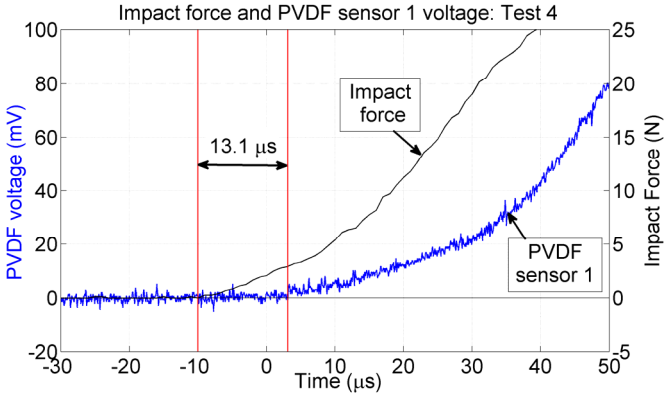


**Figure 6. Plot of time elapsed time between the impact force and voltage output from the nearest PVDF sensor.**

## FINITE ELEMENT MODELING

### Non-Ideal Impact and Plane Wave Assumption

In the analysis of the experimental results, it was assumed that plane stress waves are created in the rod due to an impact. This is the case for an ideal impact in which a freely traveling incompressible mass impacts the rod at a known velocity with the impact force distributed uniformly over the end surface of the rod. However, for the experimental tests and the speed of sound measurement technique proposed in this paper, the impact force is applied using an impact hammer. The hammer mass is not traveling freely due to the force being applied to the handle and the impact force is not applied uniformly to the end of the rod. Thus, finite element models were created for the rod used in the experimental testing in order to evaluate the validity of the plane wave assumption and the use of a non-ideal impact. Three input cases were used to examine the assumptions: (1) non-ideal impact (experimentally measured force) applied uniformly; (2) non-ideal impact (experimentally measured force) applied non-uniformly; (3) ideal impact applied non-uniformly.

**Case (1): Non-Ideal Impact Applied Uniformly.** The actual experimental force inputs have a different force profile and longer contact time than an ideal impact. Therefore, in

order to examine the effect of the non-ideal force input alone, the rod was modeled with a rigid circular plate in contact with the end of the rod, but not fixed to it, as shown in Figure 7(a). The experimentally measured impact force shown in Figure 8 (from test 2) was applied to the rigid plate, and thus applied uniformly to the end of the rod.

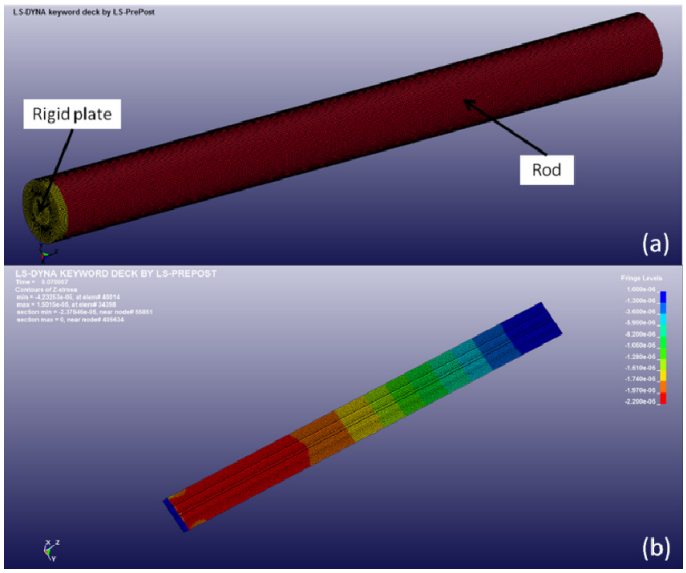


**Figure 7. (a) Finite element model for Case (1): non-ideal impact applied uniformly; (b) resulting longitudinal stresses in the cross section of the rod.**

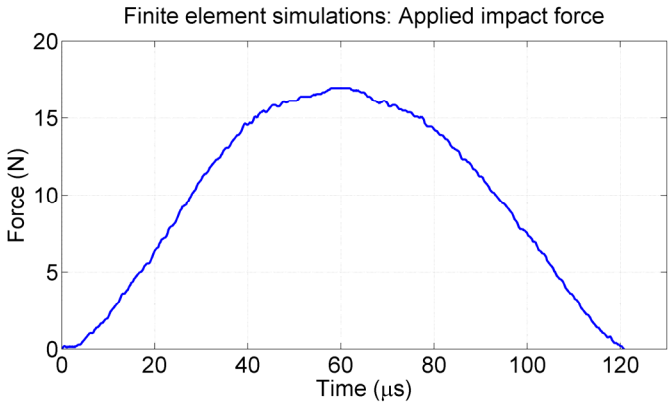


**Figure 8. Impact force that was measured experimentally and used as the non-ideal force impact for finite element model Cases (1) and (2).**

A cross section of the longitudinal stresses associated with the propagating stress wave is shown in Figure 7(b), where the cutting plane runs through the rod's axis. This figure shows that the experimental impact hammer force impact, if uniformly applied, produces a planar wave front. As a result, this verifies that the plane stress wave assumption is reasonable for non-ideal impacts.

**Case (2): Non-Ideal Impact Applied Non-Uniformly.** In this case, the same experimentally measured force input was used, but the force was applied non-uniformly to the end of the rod. This case most closely matches the actual experimental case with an impact hammer. The impacting tip of the hammer was a cylinder with a diameter of 5 mm and the hammer mass was 0.16 kg. This hammer tip was modeled with the full hammer mass and placed in contact with the end of the rod, but not fixed to it, as shown in Figure 9(a).

The experimentally measured impact force in Figure 8 was applied to the hammer tip which, like the experiment, transferred the impact force to only a small area of the end of the rod. As with the previous case, the longitudinal stresses in the rod's cross section are shown in Figure 9(b). While the stress distribution is non-uniform at short distances from the impacted end of the rod, the stress front assumes a planar shape as it propagates along the length of the rod. This validates the use of the plane wave assumption at an appropriate distance from the impacted end when a non-ideal impact is applied non-uniformly to the surface area of the rod's end.

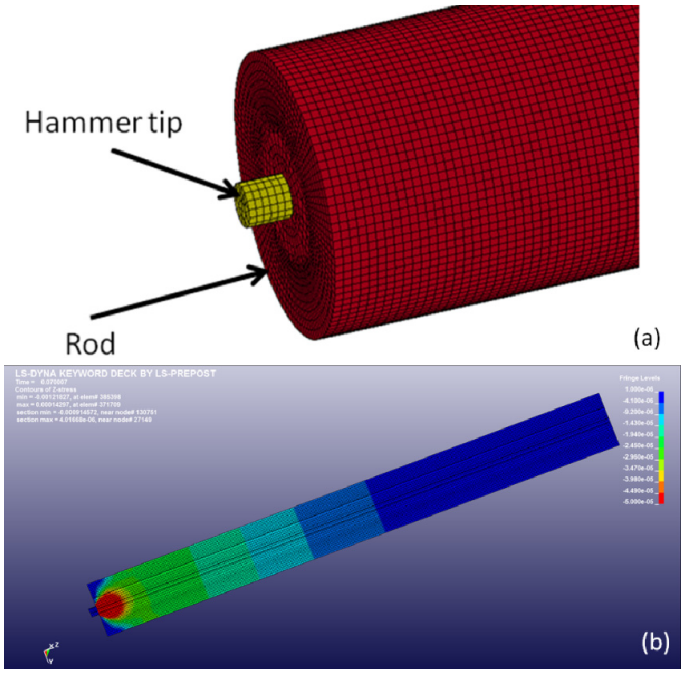


**Figure 9. (a) Finite element model for Case (2): non-ideal impact applied non-uniformly; (b) resulting longitudinal stresses in the cross section of the rod.**

**Case (3): Ideal Impact Applied Non-Uniformly.** For comparison against Case (2), this case examines the response of the rod to an ideal impact that does not uniformly impact the entire area of the rod's end. The hammer tip was aligned with the rod's axis at a distance from the end of the rod. A velocity of 0.1 m/s was applied to the hammer tip along the axial direction such that it impacted the center of one end of the free rod.

The longitudinal stress distribution in the cross section of the rod is shown in Figure 10(a), which shows that the stress distribution is irregular near the impacted end of the rod. This may be attributed to the non-symmetric element geometry in

the finite element model of the rod. This element geometry and the longitudinal stress distribution at the impacted end of the rod are shown in Figure 10(b). Despite the irregularity in the model's elements and non-uniformity of the stress near the impacted end, Figure 10(a) shows that the stress wave becomes approximately planar as it propagates along the rod. This validates the plane wave assumption for ideal but non-uniformly applied impacts. Note that the alternate red and blue areas in Figure 10(a) represent traveling compressive and tensile stress waves, respectively. The leading and trailing edges of the compressive stress waves are simultaneously visible on the bar for this simulation because of the shorter contact time associated with an ideal impact.

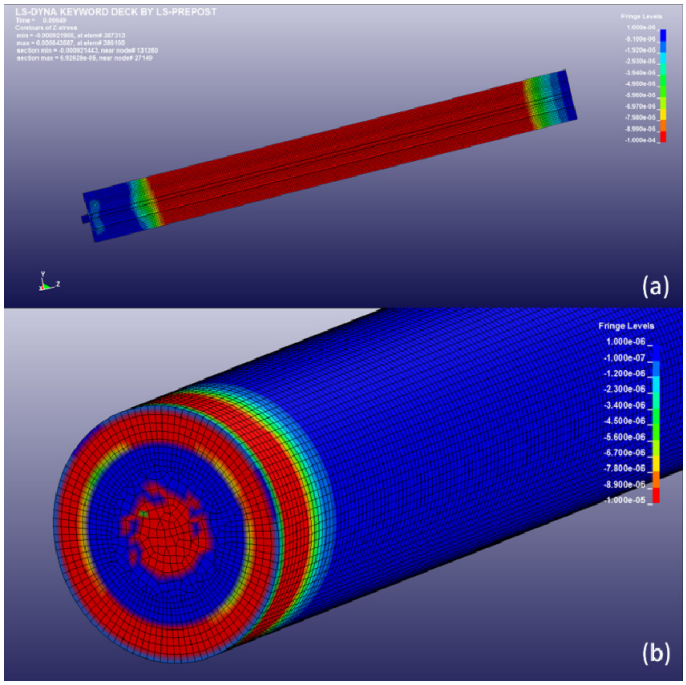


**Figure 10. Finite element model results for Case (3): ideal impact applied non-uniformly; (a) resulting longitudinal stresses in the cross section of the rod; (b) resulting longitudinal stresses in the impacted end of the rod.**

## Speed of Sound

A fourth finite element model was created to determine the speed of sound by examining the stress wave transit time between the leading edges of the two PVDF sensors shown in Figure 3. It was necessary to use a very small time step in the simulation to get adequate resolution in the transit time, but this would have greatly increased computation time for the rod model. In order to reduce the number of computations and the size of the simulation results, the rod was modeled with a reduced cross section. This is a reasonable simplification since the three finite element model cases above showed that the plane wave assumption is reasonable for non-ideal and non-uniformly applied impacts. So, as long as the structure geometry and sensor placement satisfy the requirements for the plane wave assumption, the wave propagation is one-dimensional and the rod area does not affect the response.

For the simplified model, the length was the same as the experiment, but the cross-sectional area was reduced to 0.2 mm x 0.2 mm, as shown in Figure 11. The non-ideal experimental force input in Figure 8 was scaled by the ratio of the reduced cross-sectional area of this model to the actual cross-sectional area of the rod. This force was uniformly applied to one end of the square rod, resulting in the same applied stress as the model Case (1).

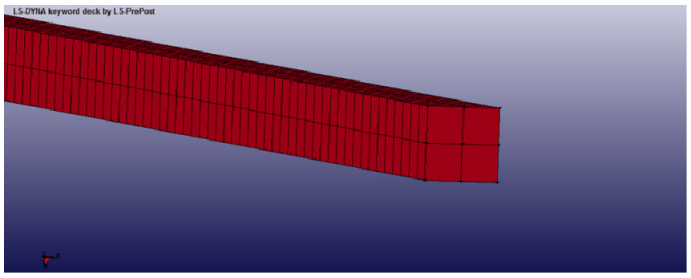

**Figure 11. Finite element model with reduced cross-sectional area for the speed of sound simulation.**

The forces acting on cross sections at the locations of the two PVDF sensors' leading edges are shown in Figure 12. The wave transit time was calculated as the difference between the time instants when force became non-zero at the two sensors' leading edges. The stress wave transit time was found to be 41.8 μs. Then, the speed of sound based on the finite element model was calculated as the ratio of the distance between the leading edges and the stress wave transit time. The simulated speed of sound was calculated to be 4956 m/s.

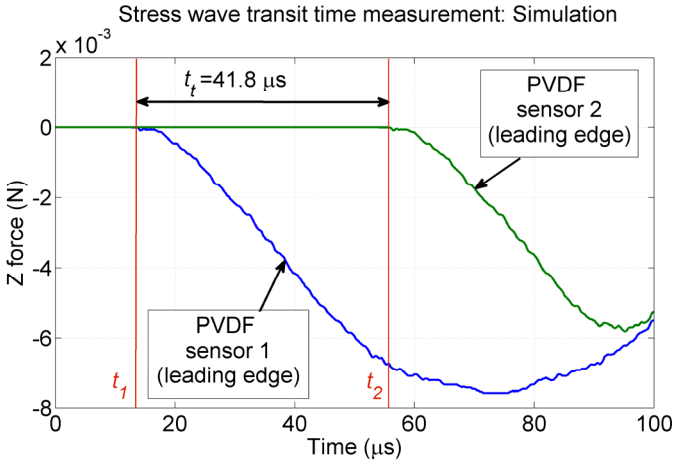


**Figure 12. Stress wave transit time measured from forces in the Z (axial) direction for the elements at the leading edges of the PVDF sensors for the speed of sound simulation.**

## DISCUSSION OF RESULTS

The average speed of the sound from the experiments as well as the speed of sound calculated using the finite element

model are summarized and compared against the theoretical analytical speed of sound for 316L stainless steel in Table 2. Both the average experimental and simulated speed of sound results are within 1% of the theoretical value. As a result, these results show that the speed of sound in solid materials can be measured with good accuracy using inexpensive PDF patch sensors which can be easily glued to the side of a structure and measured directly using an oscilloscope or other high speed data acquisition system with a high input resistance.

**Table 2. Summary of results from analytical calculations, experimental testing, and finite element modeling.**

| Method | Speed of sound in the rod [m/s] | Percentage deviation from analytical value |
|---|---|---|
| Analytical calculation | 4912 | - |
| Experimental tests | 4871 | 0.8% |
| Finite element simulation | 4956 | 0.9% |

In addition, the experimental speed of sound based on the elapsed time between the impact force and the voltage output from the nearest PVDF sensor was 5014 m/s, which represents a 2.1% deviation from the theoretical value. Despite being a very short stress wave travel distance, a very short time-of-flight, and including the region of non-planar stress waves near the impacted end, this error is low. This shows that there is no significant time lag in the PVDF sensor's response.

It should be noted that the density and elastic modulus of the 316L stainless rod were not experimentally verified and may deviate slightly from typical values. This may introduce deviations between the sample's theoretical speed of sound and the typical value used as a reference here. In addition, the speed of sound in the rod has not been yet been confirmed using more traditional and complex speed of sound measurement equipment. Therefore, more testing is required to conclusively quantify and verify the tolerances associated with the speed of sound measurement technique presented here.

## CONCLUSIONS

A straightforward method of measuring the speed of sound in solid materials and structures using two PVDF sensors and an oscilloscope was presented. By using the PVDF sensors in 31 or 32 mode to measure plane stress waves, the sensor does not need to be placed in the load path where it would be susceptible to damage and may interfere with the propagating stress wave.

The experimentally determined speed of sound in 316L stainless steel was within 0.8% of the theoretical value. It was shown that the PVDF sensors are able to accurately measure transit times on the order of microseconds and do not introduce significant measurement delays. In addition, it was shown that PVDF sensors are sensitive enough to measure the small amount of strain in the bar associated with traveling stress waves caused by low magnitude impact forces. The experimental impact force applied by the small impact hammer tip was as low as 10 N for test 3.

Finite element models of the bar showed the validity of the plane wave assumption for non-ideal and non-uniformly applied impact forces. The simulated speed of sound was found to be within 0.9% of the theoretical value.

## ACKNOWLEDGMENTS

The authors would like to acknowledge Honda R&D Americas, Inc. for their financial support of LH and KK.

## REFERENCES

[1] Kuo, I. Y., Hete, B., and Shung, K. K., 1990, "A Novel Method for the Measurement of Acoustic Speed," *The Journal of the Acoustical Society of America*, **88**(4), pp. 1679-1682.

[2] Hsu, D. K., and Hughes, M. S., 1992, "Simultaneous Ultrasonic Velocity and Sample Thickness Measurement and Application in Composites," *The Journal of the Acoustical Society of America*, **92**(2), pp. 669-675.

[3] He, P., 2000, "Measurement of Acoustic Dispersion Using Both Transmitted and Reflected Pulses," *The Journal of the Acoustical Society of America*, **107**(2), pp. 801-807.

[4] Hsu, D. K., Ayres, A. M., Guangda, M., and Guangwen, M., 1994, "Simultaneous Determination of Ultrasonic Velocity, Plate Thickness and Wedge Angle Using One-Sided Contact Measurements," *NDT & E International*, **27**(2), pp. 75-82.

[5] Obara, T., Bourne, N. K., and Mebar, Y., 1995, "The Construction and Calibration of an Inexpensive PVDF Stress Gauge for Fast Pressure Measurements," *Measurement Science and Technology*, **6**(4), pp. 345-348.

[6] Zhu, W. H., Yu, T. X., and Li, Z. Y., 2000, "Laser-Induced Shock Waves in PMMA Confined Foils," *International Journal of Impact Engineering*, **24**(6–7), pp. 641-657.

[7] Peyre, P., Berthe, L., Fabbro, R., and Sollier, A., 2000, "Experimental Determination by PVDF and EMV Techniques of Shock Amplitudes Induced by 0.6-3 ns Laser Pulses in a Confined Regime with Water," *Journal of Physics D: Applied Physics*, **33**(5), pp. 498-503.

[8] Bauer, F., 2002, "Ferroelectric PVDF Polymer for High Pressure and Shock Compression Sensors," *Proc. Proc. 11th International Symposium on Electrets, 2002. ISE 11*, pp. 219-222.

[9] Timoshenko, S., and Goodier, J. N., 1970, *Theory of Elasticity*, McGraw-Hill, New York.

[10] van Hoof, J. F. A. M., 1994, "One- and Two-Dimensional Wave Propagation in Solids," Technical Report No. 94-055.

[11] 1999, "Piezo Film Sensors Technical Manual," Measurement Specialities, Inc., Norristown, PA.

 